A New Integrated Method for Characterizing Surface Energy Heterogeneity from a Single Adsorption Isotherm

Xiandong Liu,[†] Xiancai Lu,*[,†] Qingfeng Hou,[‡] Zhijun Lu,[†] Kan Yang,[†] Rucheng Wang,[†] and Shijin Xu[†]

State Key Laboratory of Mineral Deposit Research, Department of Earth Sciences, Nanjing University, Nanjing 210093, and Beijing SJ Environmental Protection And New Material Co., Ltd., Beijing 100080, P. R. China

Received: December 24, 2004; In Final Form: April 21, 2005

To characterize surface energy heterogeneity of fine particles, this paper presents an integrated strategy from a single adsorption isotherm. By coupling the well-known integral equation method and derivative isotherm summation (DIS) procedure based on a patchwise model, the newly proposed strategy could calculate adsorption energy distributions (AEDs) for different surface patches. Correspondingly, the surface heterogeneity of materials can be described by weighted summation of patch AEDs, that is, the total AED. The validity of this new method is confirmed by both tests of rutile nanoparticles and multiwalled carbon nanotubes (MWNTs). The total AED obtained by the new method agrees well with the result from solving the integral equation directly, and it shows that AED peaks can be assigned to specific energy patches of real surface exactly. Furthermore, a detailed comparison showed that some artificial oscillation in the results can be identified with the new strategy, and the patches with low area and high surface energy could be characterized as well. In conclusion, this strategy constructs a correspondence between derived AEDs and different patches of real surface, so it will be more effective to understand surface heterogeneity by using the adsorption probe method.

1. Introduction

Surface energy heterogeneity is a fundamental property of real solids, which concerns many physics−chemistry processes, such as crystal growth, aggregation and dispersion, chemical reaction, and adsorption. It originates generally from crystallographic faces, defects and steps, chemical impurities and functional groups, and various pore structures.[1] It is proposed that quantitative information of surface heterogeneity can be extracted from adsorption isotherms of gas molecules,[1−3] and so far, many mathematical methods have been developed and well-established in the past decade.[1,2]

In the methods based on adsorption isotherm, adsorption energy distribution (AED), marked by $F(U)$, is expressed as a differential distribution of the number of adsorption sites among the values of adsorption energy U, and it is commonly normalized to unity.[1] In other words, $F(U)\,\mathrm{d}U$ represents the fraction of the sites with adsorption energies between U and $U + \mathrm{d}U$. Notably, AED could not present an absolute surface energy of an adsorbent, for it is derived from adsorption isotherm data, which is just a record of the adsorption process occurring at the solid−gas interface. Therefore, the AED is intimately dependent on a given adsorbent/adsorbate system.

A direct method for AED calculation is to employ a theoretical local adsorption model $\theta_l(p, U)$ and express the experimental adsorption isotherm $\theta(p)$ by an integral form as a linear Fredholm equation of the first kind.

$$\theta(p) = \int_{\Delta} \theta_l(p, U)\, F(U)\, \mathrm{d}U \tag{1}$$

where Δ is the integration range and $F(U)$ is the wanted AED. Thence, it is obvious that AED can be reached from eq 1. Because of its well-known ill-posedness,[4] many analytic and numeric algorithms have been developed to get a stable solution.[1] The validity of the regularization algorithm with singular value decomposition has been discussed widely[5−11] and confirmed by a wide scope of practical applications.[12−17]

Another important method characterizing energy heterogeneity assumes that real surfaces commonly consist of several types of patches with different energy states, that is, the patchwise model.[1,2] In this view, adsorption isotherm $\theta(p)$ can be written as

$$\theta(p) = \sum_{i=1}^{N} A_i \theta_i(p) \tag{2}$$

where N denotes the number of patches included, $\theta_i(p)$ stands for the local adsorption isotherm on the patch i. A_i represents the contribution of patch i and fulfills normalization condition, that is, $\sum_{i=1}^{N} A_i = 1$. Because there are even more unknown variables in eq 2, Villieras et al. proposed an effective method named DIS (derivative isotherm summation) procedure, which has been proven successful to decompose the derivative curve $\partial\theta(p)/\partial \ln(p)$ into several domains.[18,19] Each domain corresponds to one type of energetic patch of the studied surface. Meanwhile, energy heterogeneity of every patch is acquired, including characteristic energy, variance of local distribution, lateral interaction between adsorbates, and the monolayer adsorption amount on this patch.

Although the integration equation method can give a general profile of surface energetic heterogeneity as a whole, the resultant AED is poorly related with specific energy surface, that is, it is difficult to assign AED peaks to different energy patches of surface. In this paper, an integrated strategy com-

* Corresponding author. E-mail: xcljun@nju.edu.cn. Phone: +86 25 83594664. Fax: +86 25 83686016.
[†] Nanjing University.
[‡] Beijing SJ Environmental Protection And New Material Co., Ltd..

10.1021/jp044135t CCC: $30.25
Published on Web 08/04/2005

bining DIS and regularization method is proposed to study a solid surface consisting of patches with different surface energy states, such as in most minerals, where surface energy differs from one crystal face to another. To characterize these solids, the patchwise model and DIS procedure are used to obtain the local adsorption isotherm for each patch first, and then, patch AEDs $F_i(U)$ are calculated by regularization method. Finally, the AED of the whole surface can be obtained by weighted summation as eq 3

$$F(U) = \sum_{i=1}^{N} A_i F_i(U) \tag{3}$$

To justify this strategy, the surface heterogeneity of two different types of materials including rutile nanocrystals and multiwalled carbon nanotubes (MWNTs) is studied in detail. Energy heterogeneity is characterized exactly by patch AEDs. Total AEDs are calculated by using both the regularization method and the new strategy, and the results coincide very well. This shows that peaks of AED can be assigned to energy patches with warrant.

2. Methodology

2.1. Regularization Method. The regularization method transforms the integral equation eq 1 into the linear expression

$$\mathbf{g} = \mathbf{Af} \tag{4}$$

where **g** and **f** are one-dimensional matrices corresponding to $\theta(p)$ and the unknown $F(U)$, respectively, and **A** is a two-dimensional matrix representing the local isotherm $\theta_l(p, U)$. To solve the ill-posed problem, a second minimizing term is added to $||\mathbf{Af} - \mathbf{g}||^2$ in the regularization method

$$\min = ||\mathbf{Af} - \mathbf{g}||^2 + \gamma||W(F)||^2 \tag{5}$$

Here, γ is an adjustable parameter and $||W(F)||^2$ is a term weighing the smoothness of $F(U)$, which is generally defined as $\int_\Delta F^2(U)\, dU$. By adjusting γ interactively, a suitable compromise is achieved both in the smoothness of $F(U)$ and the calculation accuracy. Negative oscillations can be commonly observed in the resultant AEDs,[10,12] which is due to the smoothing properties of the integral equation, eq 1.[10] Increasing γ can suppress negative regions, but the error is increased meanwhile. Under this constraint, the experimental accuracy is a reasonable choice,[12] and thence, 0.001 is used here.

In this study, a Fowler−Guggenheim (FG) equation[20] is employed as $\theta_l(p, U)$, which has been proven a proper and common choice.[10,12] The mathematical expression is given as eq 6

$$\theta_{FG}(p, U) = \frac{Kp \exp(z\omega\theta_t)}{1 + Kp \exp(z\omega\theta_t)} \tag{6}$$

Here, the lateral interaction is described by the number of the nearest neighbors z and the interaction parameter ω. The term of $z\omega\theta_t$ denotes the average force field acting on the molecule caused by the nearest adsorbed molecules. $z = 2$ and $\omega/k = 95K$ are taken in this paper.[12] K stands for the Langmuir constant

$$K = K^0(T) \exp\left(\frac{U}{kT}\right) \tag{7}$$

The preexponential factor $K^0(T)$ can be estimated according to the Adamson method[21,22]

$$K^0(T) = \frac{N_0 \sigma^0 \gamma^0}{(2\pi MRT)^{1/2}} \tag{8}$$

Here, N_0 is Avogadro's number, σ^0 denotes the actual area per gas molecule (e.g., 0.162 nm^2 for nitrogen), γ^0 represents Frenkel's characteristic adsorption time, which is assumed to be 10^{-13} s, and M stands for the molecular weight of adsorbate gas.

2.2. DIS Method. The DIS method supposes that the studied surface consists of several energetic patches.[18,19] The number of adsorption sites on each patch yields a certain distribution with respect to adsorption energy. It is shown that fitting the derivative isotherm instead of the experimental curve is easier to distinguish local patches.[19] Both DA (Dubinin−Asthakov) and MDA (multilayer DA) models are employed as core equations to simulate the derivative isotherm for each patch with respect to the logarithm of relative pressure, the summation of which should be identified with the derivative of the experimental isotherm, that is, $\partial\theta(p)/\partial \ln(p)$. It is shown that, when fitting the derivative isotherm instead of the experiment numerical derivative, adsorption experiment values must be sufficient and accurate. Generally, the DA model holds for monolayer adsorption or micropore filling, and MDA for the multilayer adsorption or adsorption on external surfaces of porous materials, so MDA often appears after DA along relative pressure axis. For the DA model

$$\frac{\partial\theta_t}{\partial \ln(p)} = \frac{r\frac{kT}{E}[\Delta]^{r-1}\theta}{1 - \frac{r\omega}{E}[\Delta]^{r-1}\theta} \tag{9}$$

θ_t in the left-hand side denotes the resultant isotherm, and θ in the right-hand side represents DA adsorption isotherm. E is the variance of energy distribution, ω is the lateral interaction parameter, and r dominates the function shape, which is right-hand widened for $r < 3$ and left-hand widened for $r < 3$.[19] Here, Δ is a term concerning lateral interactions between adsorbate molecules

$$\Delta = \frac{kT}{E} \ln\left(\frac{p^0}{p}\right) - \frac{\omega\theta}{E} \tag{10}$$

In the DIS procedure, p^0 is commonly approximated to the saturated pressure p_s, but sometimes, it should be treated as a best-fit parameter.

For MDA

$$\frac{\partial\theta_t}{\partial \ln(p)} = \left[\frac{(P+1)^2 r[\Delta]^{r-1}\frac{kT}{E}}{1 - \frac{\omega}{E}r[\Delta]^{r-1}e^{-\Delta^r}} + P(P+1)\right]e^{-\Delta^r} \tag{11}$$

with

$$P = \frac{p/p_s}{1 - k'(p/p_s)} \tag{12}$$

Here, $k' = 1$ is taken. In the fitting, the local maximum of the derivative isotherm indicates the introduction of a new adsorption domain. Some other fundamental principles and iterative fitting algorithms are discussed in detail in published articles.[18,19]

2.3. Integrated Strategy. Since DIS fitting extracts the derivative isotherm of each patch, the patch adsorption isotherm

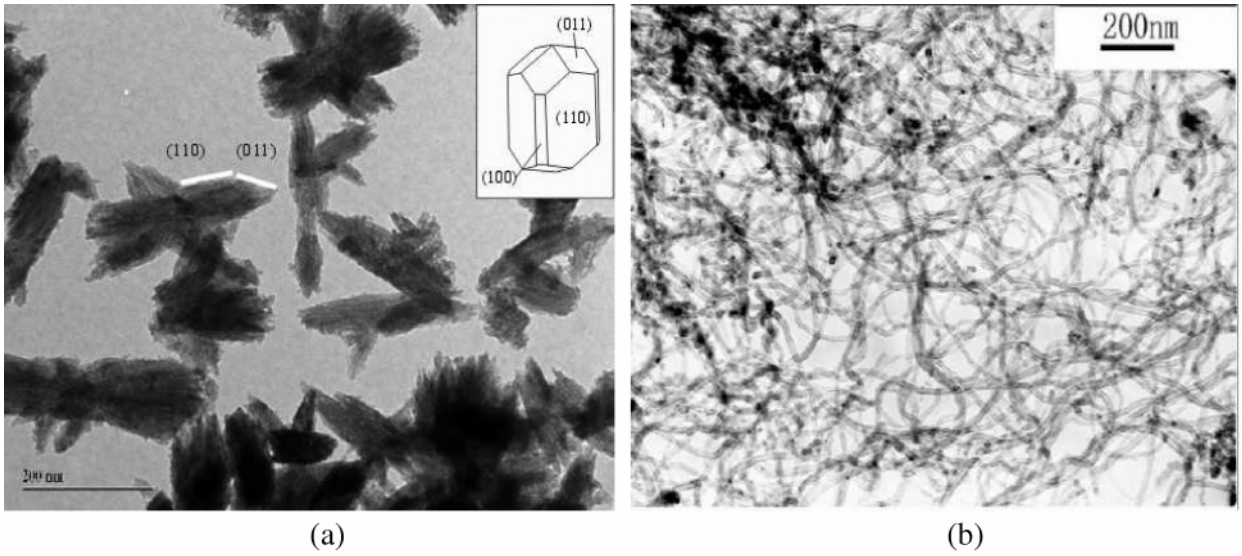

Figure 1. TEM images of experimental samples: (a) rutile and (b) MWNTs.

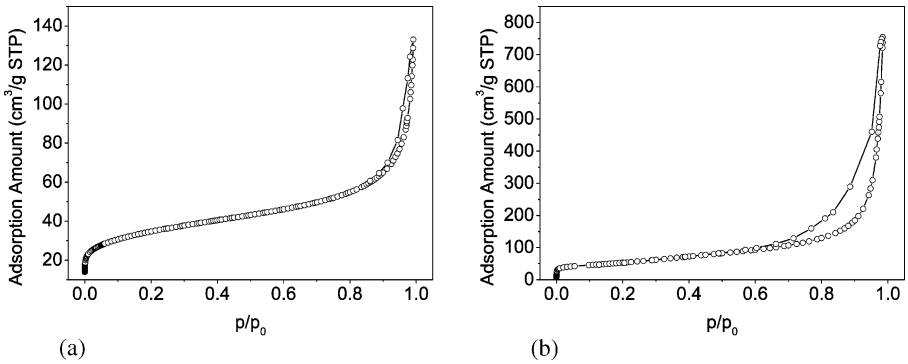

Figure 2. Adsorption isotherms of experimental samples: (a) rutile and (b) MWNTs.

can be recovered by an integrating approach, and here, the cumulative trapezoidal method is employed.

Then, under the assumption that the number of different adsorption sites on each patch yields a certain distribution, the patch isotherm can be expressed by a formula analogous to eq 1[1,19]

$$\theta_i(p) = \int_{\Delta}\theta_{il}(p, U)\, F_i(U)\, \mathrm{d}U \tag{13}$$

Here, the regularization method is used to solve eq 13, and the patch AED (i.e., $F_i(U)$) is acquired. $F_i(U)$ characterizes the energy heterogeneity of the individual energetic patch. So far, the patch AED $F_i(U)$) is calculated, the fractional contribution of patch *i*, *Ai*, is given by DIS fitting, and the next step is to evaluate the total AED. For a patchwise surface, we can import eqs 1 and 13 into eq 2, and then

$$\int_{\Delta}\theta_i(p, U)\, F(U)\, \mathrm{d}U = \sum_{i=1}^{N} A_i \int_{\Delta}\theta_{il}(p, U)\, F_i(U)\, \mathrm{d}U \tag{14}$$

Because the FG equation (eq 6) is selected as the local theoretical isotherm, eq 14 is rewritten as

$$\int_{\Delta}\theta_{\mathrm{FG}}(p, U)\, F(U)\, \mathrm{d}U = \int_{\Delta}\theta_{\mathrm{FG}}(p, U)[\sum_{i=1}^{N} A_i F_i(U)]\, \mathrm{d}U \tag{15}$$

Then, eq 3 is derived, and the resultant $F(U)$ satisfies the normalization condition obviously.

In summary, the flow of this strategy includes the sequential steps: (1) obtaining derivative isotherms of patches from a single experimental isotherm using DIS fitting, (2) recovering the patch isotherms, (3) calculating the patch AED with the regularization algorithm, (4) evaluating the total AED according to eq 3 and assigning each peak to corresponding patch.

3. Experiment Section

3.1. Samples. The two samples are both lab-synthesized, and TEM images (JEM-1230) are shown in Figure 1. The particle size of rutile ranges ~100−200 nm, where two kinds of crystallographic faces, (110) and (011), are distinguishable and marked in Figure 1a. It is hard to distinguish the (100) faces in the TEM image (Figure 1a), because they often exhibit as long and narrow rectangles and are shaded by the projection of (110). The diameter of the MWNTs is about 20−40 nm.

3.2. Adsorption Isotherms Measurement. Adsorption isotherms were measured on a Micromeritics ASAP-2010 volumetric adsorption analyzer (Norcross, GA) at 77.5 K and high-purity (99.999%) nitrogen as the probing adsorbate. The adsorption quantity was recorded as a function of relative pressures from below 10^{-6} to the saturation pressure p_0. To get accurate data in the low-pressure region, the maximum equilibration time was set 1 h according to Bereznitski et al.[17] Prior to measurements, samples are outgassed to below 0.02 Pa for more than 10 h at 423 K. Adsorption isotherms are illustrated in Figure 2. In this study, the relative pressure is selected below 0.14, and this range is adequate for both the regularization method and DIS.[12,18]

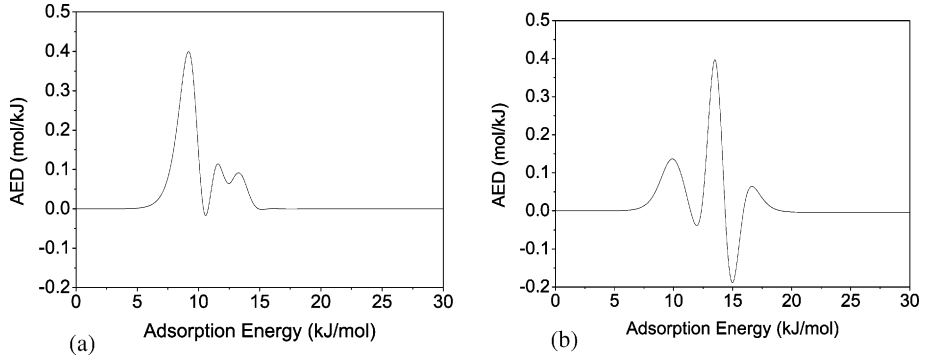

Figure 3. AEDs calculated using the regularization method with $\gamma = 0.001$: (a) rutile and (b) MWNTs.

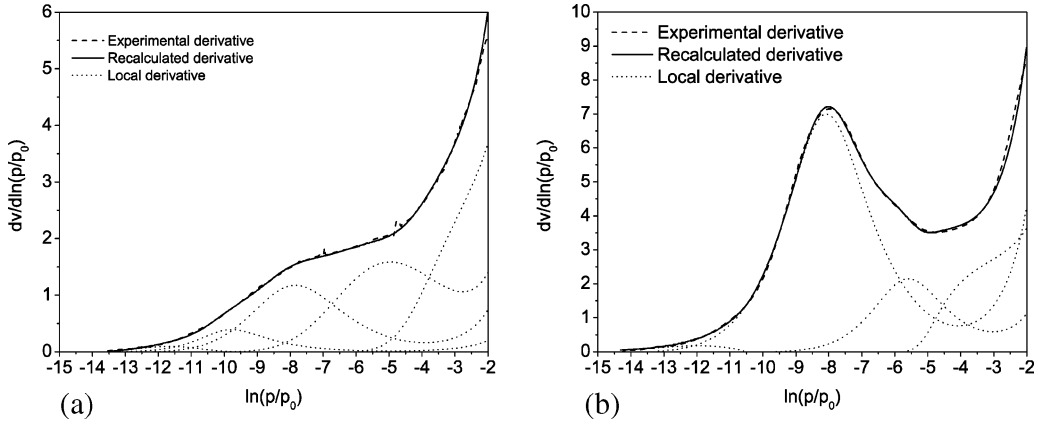

Figure 4. Derivative nitrogen adsorption isotherms decomposed using DIS procedure: (a) rutile and (b) MWNTs.

TABLE 1: Parameters Adjusted to the Experimental N_2 Derivative Isotherm of Rutile[a]

domain	model	r	$\ln(p^0/p_s)$	ω/kT	E/kT	V_m (cm^3/g)	S_{ssa} (m^2/g)	A
1	DA	3.0	−9.5	0	2.50	0.20	0.87	0.011
2	MDA	6.0	0	1.4	9.45	1.11	4.83	0.060
3	MDA	4.6	0	1.0	7.80	4.11	17.88	0.221
4	MDA	3.7	0	0	5.50	6.00	26.10	0.322
5	MDA	3.0	0	−0.7	3.00	7.19	31.28	0.386

[a] V_m is the monolayer adsorption amount on the corresponding domain; S_{ssa} is the specific surface area obtained from the V_m, where the cross-sectional area of nitrogen is assumed to be 0.162 nm^2. A, the contribution of the individual domain to the total adsorption (defined in eq 2), is calculated from the fraction of the total specific area for each domain.

TABLE 2: Parameters Adjusted to the Experimental N_2 Derivative Isotherm of MWNTs[a]

domain	model	r	$\ln(p^0/p_s)$	ω/kT	E/kT	V_m (cm^3/g)	S_{ssa} (m^2/g)	A
1	DA	1.8	−10.5	0	2.30	0.50	2.18	0.005
2	MDA	3.8	0	2.0	7.73	23.70	103.1	0.624
3	MDA	3.6	0	1.2	5.50	5.90	25.67	0.155
4	MDA	5.5	0	−1.7	3.90	8.20	35.67	0.216

[a] V_m is the monolayer adsorption amount on the corresponding domain; S_{ssa} is the specific surface area obtained from the V_m, where the cross-sectional area of nitrogen is assumed to be 0.162 nm^2. A, the contribution of the individual domain to the total adsorption (defined in eq 2), is calculated from the fraction of the total specific area for each domain.

4. Results

4.1. Regularization AEDs. Shown in Figure 3 are the AEDs of rutile and MWNTs calculated using the regularization method with $\gamma = 0.001$. It is clear that three peaks are exhibited for rutile. In quantity, the low-energy peak is dominant and the other two almost equal. For the case of MWNTs, three peaks are also observed, but different from the AED of rutile, the high-energy peak at ~12.5−14.0 kJ/mol is the dominant one.

4.2. DIS Domains. The DIS fitting results of rutile and MWNTs are presented in Figure 4 together with the corresponding data listed in Table 1 and Table 2, respectively. The derivative isotherm of rutile is decomposed into five domains and that of MWNTs into four. As shown in Figure 4, the resultant derivative isotherms fit well to the experimental ones.

4.3. Integrated Strategy Results. Figures 5 and 6 present the patch AEDs of rutile and MWNT domains calculated by the regularization method with $\gamma = 0.001$. Because the calculation is limited on specific patches, these results are devoted to characterizing adsorption energy of the corresponding patches, and together, they represent energy heterogeneity of the whole surface.

The AEDs calculated using the regularization method and the integrated strategy are presented in dashed and solid lines in Figure 7, named regularization AED and integrated AED, respectively. It is indicated that those oscillations shown in Figures 5 and 6 are suppressed evidently in integrated AEDs, because they are counteracted in the calculation of eq 3.

5. Discussions

The good agreement shown in Figure 7a between the regularization AED and the integrated AED proves the validity of the integrated strategy. However, there is still a small difference in that peak 4 and peak 5 in the integrated AED of rutile are absent in the regularization AED (Figure 7a). As for MWNTs shown in Figure 7b, a general agreement between both AEDs is exhibited except for the absence of peak 4 and a small shift in peak positions. Additionally, the strong oscillations in the regularization AED of MWNTs are suppressed evidently

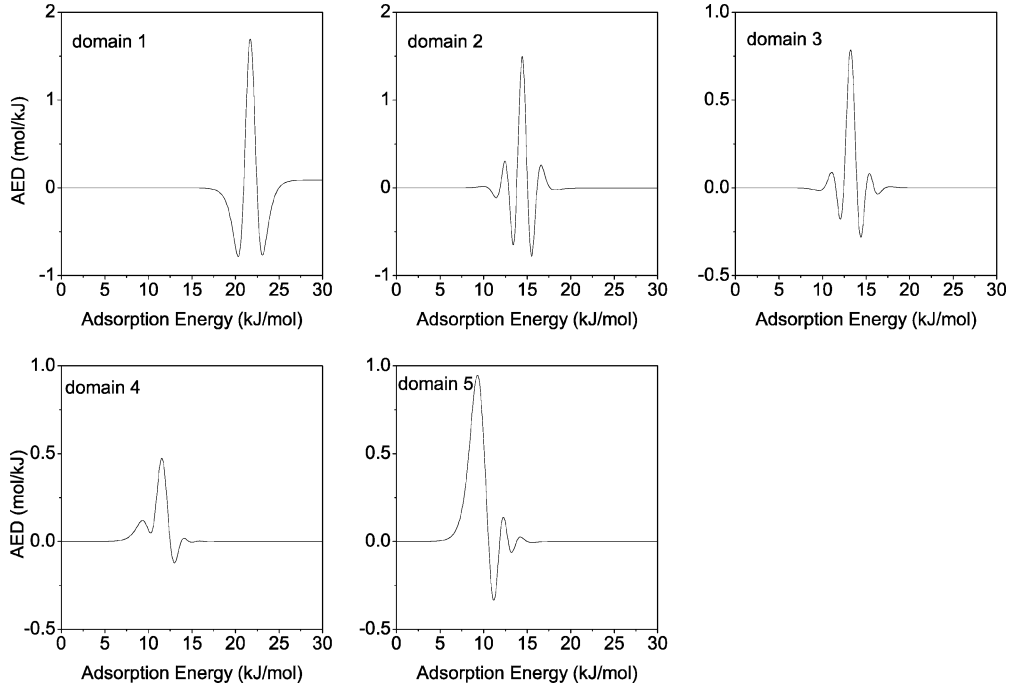

Figure 5. Patch AEDs of the rutile corresponding to the domains decomposed using DIS.

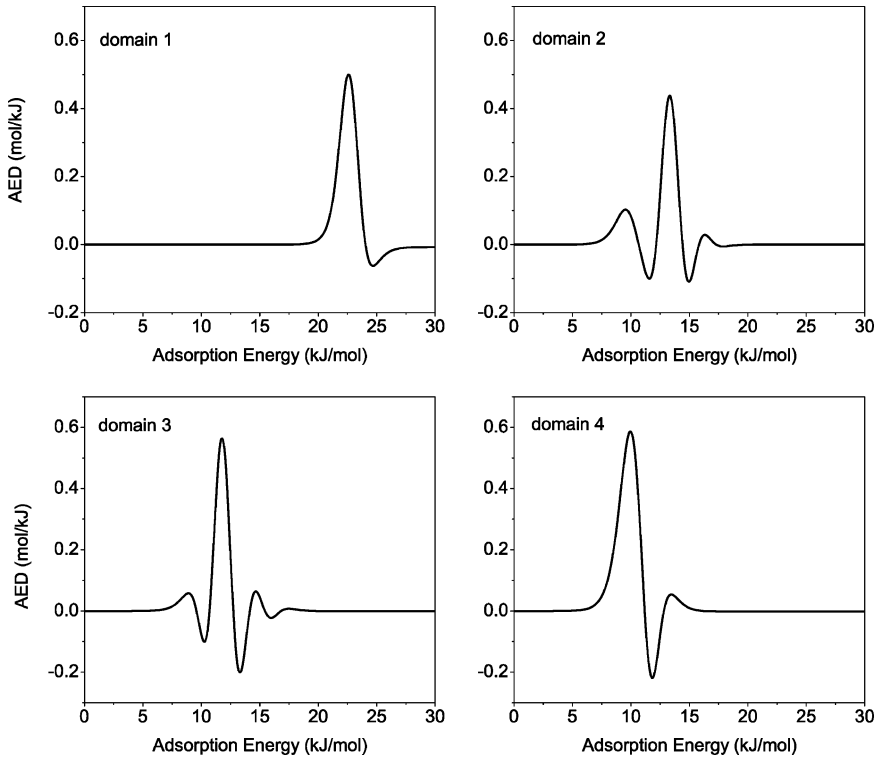

Figure 6. Patch AEDs of the MWNTs corresponding to the domains decomposed using DIS.

in the integrated AED, and thence, the latter is thought to be more stable and credible than the former.

The agreement between the two AEDs also suggests that peaks of the regularization AED can be assigned to specific energetic patches. Since the integrated AED is obtained from the linear weighed summation of eq 3, the contribution of each individual domain to the total AED can be estimated, that is, to which domain the peak can be assigned according to peak position. The assignment results of both samples are listed in Tables 3 and 4. The coincidence between regularization AED and integrated AED, which just reflects the adsorption energy distribution in the same adsorbate/adsorbent system ,in principle, confirms that the assignment of regularization AED peaks to specific energetic domains acquired by DIS fitting is feasible. In the case of rutile, peak 1, peak 2, and peak 3 can be assigned to three kinds of faces: (110), (100), and (011) (shown as inset in Figure 1a), respectively. Under the current assignment, their corresponding surface energies are relatively consistent with ab initio calculations,[23] and the contribution of the individual domain to the total adsorption agrees qualitatively with that of different surfaces to total specific surface area.[24,25] Thence, adsorption energy on (110), (100), and (011) is described by domains 5, 4, and 3, respectively. As for the regularization AED of MWNTs, the right-hand peak denoted as peak 3 corresponds

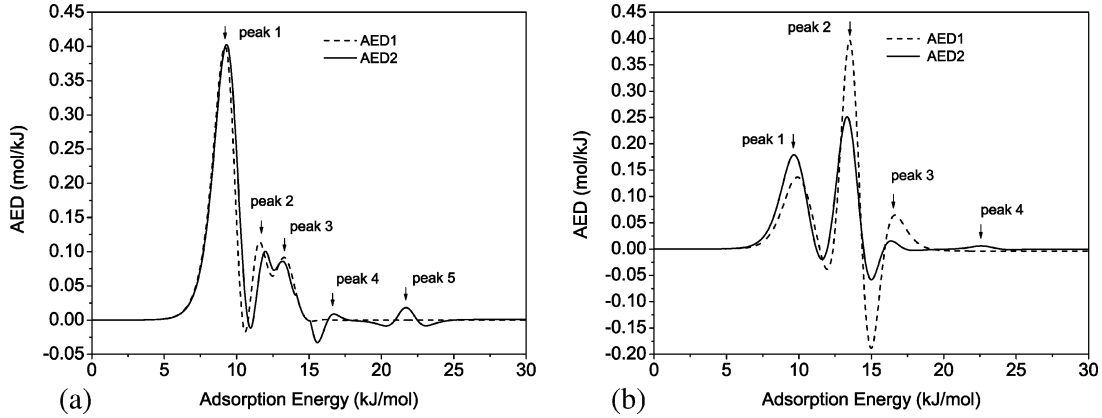

Figure 7. The AEDs obtained with both methods: (a) rutile and (b) MWNTs. The peaks are named after Arabic numerals and marked with black arrows in the figure. AEDI: regularization AED; AED2: integrated AED.

TABLE 3: Assignment of Peaks in the AED of Rutile[a]

integrated AED	peak 1 (5.0, 11.0)	peak 2 (11.5, 13.0)	peak 3 (12.5, 15.0	peak 4 (16.5, 17.5)	peak 5 (21.0, 22.5)
patch AEDs	$F_5(U)$ (5.0, 10.5)	$F_4(U)$ (10.0, 12.5)	$F_3(U)$ (12.5, 14.0) $F_2(U)$ (14.0, 15.0)	righthand oscillation of $F_2(U)$ (16.5, 17.5)	$F_1(U)$ (21.0, 22.5)
regularization AED	peak 1 (5.0, 10.5)	peak 2 (11.0, 13.0)	peak 3 (12.5, 15.0)		

[a] The peak *n* is the same as that marked in Figure 7a, and $F_i(U)$ means the patch AED on the domain *i*, shown in Figure 5. In the parentheses are the spans.

TABLE 4: Assignment of Peaks in the AED of MWNTs[a]

integrated AED	peak 1 (6.0, 11.5)	peak 2 (12.0, 14.0)	peak 3 (16.0, 17.5)	peak 4 (20.0, 24.0)
patch AEDs	$F_4(U)$ (6.0, 11.5)	$F_2(U)$ (12.5, 14.0) $F_3(U)$ (11.5, 12.5)	righthand oscillation of $F_3(U)$ (16.0, 17.5)	$F_1(U)$ (20.0, 24.0)
regularization AED	peak 1 (6.0, 11.5)	peak 2 (12.5, 14.0)	peak 3 (16.0, 19.0)	

[a] The peak *n* is the same as that marked in Figure 7b, and $F_i(U)$ means the patch AED on the domain *i*, shown in Figure 6. In the parentheses are the spans.

to peak 3 of the integrated AED, which may have resulted from a weak oscillation in the patch AED of domain 3, so it is thought to be of no physical meaning. The major peaks, peak 1 and peak 2, are distinguished distinctly and suggest the existence of two types of energetic surfaces. It has been proven that the surface of MWNTs generally consists of two energy states of carbon (i.e., graphite-like and disordered carbon), and the surface energy of graphite-like carbon is lower than that of disordered carbon.[26] Accordingly, peak 1, the lower-energy peak, was assigned to graphite-like carbon, and peak 2, the high-energy one, to disordered carbon. Although these adsorption sites may distribute unlike regular crystal faces, they can be probed with respect to adsorption energy.

Comparison between regularization AED and integrated AED provides detailed information concerning the small peaks in AEDs. According to the peak assignment, it can be interpreted that the absence of some integrated AED peaks (peak 4 and peak 5 for the rutile; peak 4 for the MWNTs) in regularization AED is attributed to the small contribution of corresponding patches to the total AEDs, and consequently, they are suppressed in the calculation of regularization AED. However, they are reserved in integrated AED, because the calculation (i.e., eq 3) is only a summation operation. It is noteworthy that peak 5 of rutile, as well as peak 4 of MWNTs in integrated AED has resulted from the high-energy adsorption sites of samples, which may be caused by micropores or defects.

6. Conclusions

In this paper, an integrated strategy based on a single adsorption isotherm is proposed to study surface energy heterogeneity quantitatively, which is confirmed by two case studies including rutile nanoparticles and MWNTs. Specific energy patches on real surfaces can be characterized by derived patch AEDs from this strategy. Total AED, for example, integrated AED, is also calculated, and its agreement with regularization AED demonstrates that peaks of AED could be assigned to specific patches. Meanwhile, the pseudo-information in regularization AED means that some oscillation could be detected, evaluated, and thence excluded. In addition, some small peaks originating from those surfaces with relatively small surface area and high surface energy may be omitted in regularization AED but can be shown in integrated AED. In summary, according to applying the new strategy, a comprehensive and exact correspondence is constructed between AED and the underlying surface, so study on surface energy heterogeneity can be facilitated.

Acknowledgment. This work was supported by the National Science Foundation of China under grant nos. 40003002 and 40373024. The authors acknowledge Professor Zhang Huiliang and Dr. Wu Qiang from Nanjing University for providing the samples, Engineer Wang Chunzhao for her kind help in TEM observation in Nanjing Institute of Geology and Palaeontology, Chinese Academy of Sciences.

References and Notes

(1) Jaroniec, M.; Madey, R. *Physical Adsorption on Heterogeneous Solids*; Elsevier: Amsterdam, 1988.

(2) Rudziński, W.; Everett, D. H. *Adsorption of Gases on Heterogeneous Surfaces*; Academic Press: London, 1991.
(3) Françoise, R.; Jean, R.; Kenneth, S. *Adsorption by Powders and Porous Solids*; Academic Press: London, 1999.
(4) Phillips, D. L. *J. Assoc. Comput. Mach.* **1962**, *9*, 84.
(5) House, W. A. *J. Colloid Interface Sci.* **1978**, *67*, 166.
(6) Merz, P. H. *J. Comput. Phys.* **1980**, *38*, 64.
(7) Papenhuijzen, J.; Koopal, L. K. In *Adsorption from Solutions*; Ottewill, R. H., Rochester, C. H., Smith, A. L., Eds.; Academic Press: London, 1983; p 211.
(8) Brown, L. E.; Travis, B. J. In *Fundamentals of Adsorption*; Myers, A. L., Belfort, G., Eds.; American Institute of Chemical Engineers: New York, 1984; p 125.
(9) Britten, J. A.; Travis, B. J.; Brown, L. F. *AIchE Symp. Ser*. **1983**, *79*, 1.
(10) Szombathely, M. v.; Brauer, P.; Jaroniec, M. *J. Comput. Chem.* **1992**, *13*, 17.
(11) Jagiello, J. *Langmuir* **1994**, *10*, 2778.
(12) Heuchel, M.; Jaroniec, M.; Gilpin, R. K.; Brauer, P.; Szombathely, M. v. *Langmuir* **1993**, *9*, 2537.
(13) Jagiello, J.; Bandosz, T. J.; Schwarz, J. A. *Langmuir* **1997**, *13*, 1010.
(14) Choma, J.; Jaroniec, M. *Langmuir* **1997**, *13*, 1026.
(15) Jaroniec, C. P.; Kruk, M.; Jaroniec, M.; Sayari, A. *J. Phys. Chem. B* **1998**, *102*, 5503.
(16) Li, Z. J.; Kruk, M.; Jaroniec, M.; Ryu, S. K. *J. Colloid Interface Sci.* **1998**, *204*, 151.
(17) Bereznitski, Y.; Gangoda, M.; Jaroniec, M.; Gilpin, R. K. *Langmuir* **1998**, *14*, 2485.
(18) Villiéras, F.; Cases, J. M.; Francois, M.; Michot, L. J.; Thomas, F. *Langmuir* **1992**, *8*, 1789.
(19) Villiéras, F.; Michot, L. J.; Bardot, F.; Cases, J. M.; Francois, M.; Rudzinski, W. *Langmuir* **1997**, *13*, 1104.
(20) Fowler, R. H.; Guggenheim, E. A. *Statistical Thermodynamics*; Cambridge University Press: London, 1949.
(21) Adamson, A. W.; Ling, I. *Adv. Chem. Ser*. **1961**, *33*, 51.
(22) Adamson, A. W. *Physical Chemistry of Surfaces*; Wiley: New York, 1990.
(23) Ramamoorthy, M.; Vanderbilt, D.; King-Smith, R. D. *Physical Review B* **1994**, *49*, 16721.
(24) Diebold, U. *Surf. Sci. Rep.* **2003**, *48*, 53.
(25) Bakaev, V. A.; Steele, W. A. *Langmuir* **1992**, *8*, 1372.
(26) Allaoui, A.; Bai, S.; Cheng, H. M.; Bai, J. B. *Compos. Sci. Technol.* **2002**, *62*, 1993.